The steroid derivative 6-aminocholestanol inhibits the DEAD-box helicase eIF4A (LieIF4A) from the Trypanosomatid parasite Leishmania by perturbing the RNA and ATP binding sites

Yosser Zina Abdelkrim, Emna Harigua-Souiai, Mourad Barhoumi, Josette Banroques, Arnaud Blondel, Ikram Guizani, N. Kyle Tanner

The steroid derivative 6-aminocholestanol inhibits the DEAD-box helicase eIF4A (LieIF4A) from the Trypanosomatid parasite *Leishmania* by perturbing the RNA and ATP binding sites

Yosser Zina Abdelkrim[1,2,3], Emna Harigua-Souiai[2], Mourad Barhoumi[2], Josette Banroques[1], Arnaud Blondel[4], Ikram Guizani[2*], N. Kyle Tanner[1*]

[1] Expression Génétique Microbienne, CNRS UMR8261/Université Paris Diderot-Paris 7 & Paris Sciences et Lettres Research University, Institut de Biologie Physico-Chimique, 13 rue Pierre et Marie Curie, 75005 Paris, France

[2] Molecular Epidemiology and Experimental Pathology (LR16IPT04), Institut Pasteur de Tunis/Université de Tunis el Manar, 13 Place Pasteur, BP74 Tunis-Belvédère, 1002 Tunisia

[3] Faculté des Sciences de Bizerte, Université de Carthage, 7021 Zarzouna-Bizerte, Tunisia.

[4] Unité de Bioinformatique Structurale, CNRS UMR 3528, Département de Biologie Structurale et Chimie, Institut Pasteur, 25-28 rue du Dr Roux, 75015 Paris, France.

* Corresponding author.
E-mail address: kyle.tanner@ibpc.fr (N.K. Tanner)
CNRS UMR8261, IBPC, 13 rue Pierre et Marie Curie, 75005, Paris, France

* Correspondence can also made to:
E-mail address: ikram.guizani@pasteur.ms.tn (I. Guizani)
Molecular Epidemiology and Experimental Pathology (LR16IPT04), Institut Pasteur de Tunis/Université de Tunis el Manar, 13 Place Pasteur, BP74 Tunis-Belvédère, 1002 Tunisia

Abbreviations: ATP, adenosine 5'-triphosphate; BSA, bovine serum albumin; CL, cutaneous leishmaniasis;; DMSO, dimethyl sulfoxide; $eIF4AI_{Mus}$, mouse translation initiation factor eIF4AI; EDTA, ethylenediaminetetraacetic acid; Gp32, bacteriophage T4 gene 32; LieIF4A, *L. infantum* translation initiation factor 4A;; RecA, recombinant protein A;; Tris-HCl, Tris(hydroxymethyl)aminomethane hydrochloride; VL, visceral leishmaniasis.

Abstract

The antifungal agent 6-aminocholestanol targets the production of ergosterol, which is the principle sterol in many fungi and protozoans; ergosterol serves many of the same roles as cholesterol in animals. We found that it also is an effective inhibitor of the translation-initiation factor eIF4AI from mouse ($eIF4AI_{Mus}$) and the Trypanosomatid parasite *Leishmania* (LieIF4A). The eIF4A proteins belong to the DEAD-box family of RNA helicases, which are ATP-dependent RNA-binding proteins and RNA-dependent ATPases. DEAD-box proteins contain a commonly-shared core structure consisting of two linked domains with structural homology to that of recombinant protein A (RecA) and that contain conserved motifs that are involved in RNA and ATP binding, and in the enzymatic activity. The compound inhibits both the ATPase and helicase activities by perturbing ATP and RNA binding, and it is capable of binding other proteins containing nucleic acid-binding sites as well. We undertook kinetic analyses and found that the *Leishmania* LieIF4A protein binds 6-aminocholestanol with a higher apparent affinity than for ATP, although multiple binding sites were probably involved. Competition experiments with the individual RecA-like domains indicate that the primary binding sites are on RecA-like domain 1, and they include a cavity that we previously identified by molecular modeling of LieIF4A that involve conserved RNA-binding motifs. The compound affects the mammalian and *Leishmania* proteins differently, which indicates the binding sites and affinities are not the same. Thus, it is possible to develop drugs that target DEAD-box proteins from different organisms even when they are implicated in the same biological process.

Keywords (5): *Leishmania infantum*; drug design; hippuristanol; RNA helicase; translation-initiation factor

1. Introduction

Leishmaniases are neglected tropical diseases caused by the Trypanosomatid parasite *Leishmania* that affect mostly developing countries with limited public health resources. Each year it is estimated that there are around 0.7 to 1.2 million new cases of cutaneous leishmaniasis (CL) and about 0.2 to 0.4 million new cases of the most severe form of the disease, visceral leishmaniasis (VL), which is typically fatal if left untreated [1]. Leishmaniases require adequate control measures, clinical vaccines and effective drug treatments. The current drug treatment regimes for leishmaniasis have recently been reviewed [3]. They include liposomal amphotericin B (LAMB), pentavalent antimonials monotherapy and pentavalent antimonials in combination with topical agents, such as paromomycin for VL/CL, pentoxifylline or allopurinol for CL and pentoxyfylline for mucocutaneous leishmaniasis (MCL). Other systemic mono-therapies are recommended such as miltefosine for VL/CL or pentamidine for CL/MCL. Moreover, alternative combination regimens are available for CL and VL. However, these drugs are expensive and are often associated with toxicities and adverse side effects. Moreover, there is the risk of the parasites developing drug resistance. Effective vaccines against *Leishmania* are still under development [4]. Thus, there is an urgent need to develop more selective, less expensive new drugs. In this vein, we are interested in finding inhibitors of the DEAD-box helicases from *Leishmania*.

DEAD-box helicases are ubiquitous proteins that are associated with all processes involving RNA, from transcription, processing, transport, translation and to RNA decay [5, 6]. They are ancestral proteins that are found in all three kingdoms of life. *In vitro*, the characterized proteins are ATP-dependent RNA-binding proteins and RNA-dependent ATPases. Moreover, they have been shown to disrupt short RNA-RNA and RNA-DNA duplexes, albeit inefficiently [6, 7]. *In vivo*, DEAD-box proteins are highly specific and highly regulated; specificity is probably conferred by the cellular context and associated

cofactors [8]. Their importance to the cell is indicated by the large number of variants DEAD-box proteins. For example, the yeast *Saccharomyces cerevisiae* has 25 different DEAD-box helicases that are mostly essential and rarely interchangeable [9]. Humans have 36 different proteins and *L. major* has 28 [10, 11].

The DEAD-box proteins are characterized by conserved core structures consisting of two linked domains with structural homology with that of recombinant protein A (RecA). The RecA-like domains contain eleven conserved motifs that are involved in ATP and RNA binding, and in the enzymatic activity [6, 7, 12]. The Q motif is involved in adenine recognition; motifs Ia, GG, Ib, IV, QxxR and V bind the RNA; and motifs I (Walker A motif), II (Walker B motif), III, V and VI interact with the phosphoanhydride backbone of the ATP. Binding of ATP and RNA promote a "closed" conformation of the two RecA-like domains, which has a high affinity for the ligands. Hydrolysis of the ATP and subsequent phosphate release promotes an "open" conformation where the RecA-like domains are not constrained relative to one another and that have low affinity for the RNA. In addition, DEAD-box proteins have variable amino- and carboxyl-terminal extensions, as well as insertions and deletions within the core domains.

Because of their important cellular roles, these helicases are potential targets for therapeutic and prophylactic agents [13-16]. The mammalian DEAD-box proteins eIF4AI and eIF4AII, which are translation-initiation factors, have been of particular interest for screening for candidate drugs [17]. One such compound is hippuristanol. Hippuristanol is a hydroxycholestanol (a steroid derivative) isolated from the coral *Isis hippuris* [18]. It is an allosteric inhibitor of RNA binding to eIF4A most likely by locking the two RecA-like domains in an aberrant closed conformation [19]. The proposed binding site encompasses and extends beyond motifs V and VI, and it is thought to be unique to eIF4A-like proteins; as a consequence, it shows little inhibition of other tested DEAD-box proteins [19].

We previously showed that LieIF4A (*LinJ01.0780*/*LinJ01.0790*) was a probable ortholog of eIF4A in *L. infantum* (a causal species of visceral leishmaniasis), which was consistent with the results of others [20-22]. We subsequently used molecular modeling, molecular dynamics and docking simulations of LieIF4A to identify potential drug targets on the protein, and then we screened potential candidates for these sites through an analysis of the RNA-dependent ATPase activity [23]. The various compounds inhibit both LieIF4A and mouse eIF4AI ($eIF4AI_{Mus}$), although we noted that there are significant differences in the enzymatic properties. We found that the epimeric compound 6-α/ß-aminocholestanol is of particular interest; the data are consistent with it binding the RecA-like domain 1 of LieIF4A at a pocket consisting of the RNA-interacting motifs Ia, GG and Ib, and a short three-amino-acid insertion that was absent in the alignments of other DEAD-box proteins [23]. The pocket is predicted to exist only in the open conformation of the RecA-like domains, which exhibits more conformational flexibility. This result is noteworthy because the compound has significant structural similarity to hippuristanol even though the initial screening of compounds was constrained only for sites detected through the modeling. We validated the 6-aminocholestanol with experimental assays on extracellular promastigotes (IC50 = 4.1 μM) and on intramacrophage amastigotes (IC50 = 1.4 μM); it showed little toxicity on the host cell (CC50 = 43.4 μM). Thus, 6-aminocholestanol exhibited a selectivity index of 31.7, which makes it a promising anti-*Leishmania* molecule [23].

In this study, we have further characterized the effects of 6-aminocholestanol on LieIF4A, and we have made additional comparisons between LieIF4A and $eIF4AI_{Mus}$. Both the *Leishmania* and mouse proteins are sensitive to the compound but in different ways; we find that the inhibitory effects probably involve different binding pockets on the two proteins. This indicates that in principle drugs can specifically target DEAD-box proteins with the

same function from different organisms, which is desirable for the selective treatment of parasitic infections such as Leishmaniases.

2. Materials and methods

2.1. Compounds and proteins

A limited amount of the isomeric 6-aminocholestanol was obtained directly from the synthesizing laboratory [24]. It consisted of a mix of 84% 6-α-aminocholestanol and 16% 6-ß-aminocholestanol. We previously showed that the pure epimer 6-α-aminocholestanol gave similar results [23]. The compound was dissolved in ultrapure anhydrous DMSO (D2650; Sigma-Aldrich, St. Louis, MO, USA) to make stock solutions. Solutions were stored at -20°C until needed. BSA and Gp32 were obtained from Sigma-Aldrich.

2.2. Protein expression and purification

The mutant RecA-like domain 1 (1–238; D1-GAT) was amplified from the previously described K76A mutant of LieIF4A and domain 1 oligonucleotides [20, 25]. In brief, the gene was amplified with oligonucleotides LieIF2_up (5' GCG CGA CTA GTC ATA TGG CGC AGA ATG ATA AGA TCG 3'), which contained SpeI and NdeI sites, and LieIFD1_3' (5' GCG CGC TCG AGC GTC AGG CTC TCG CGC TTC 3'), which contained an XhoI site; regions of hybridization are shown underlined. The product was digested with NdeI and XhoI, purified by electrophoretic separation on a 1% agarose gel and eluted, and then it was cloned into the pET-22b (Merck-Novagen, Darmstadt, Germany) expression vector digested with the same enzymes. The final construct was verified by sequencing.

The mouse eIF4AI gene (*DDX2A*; P60843) was a gift from Patrick Linder [26]. It was similarly PCR amplified with oligonucleotides IF41_Mus_up (5' GCG CGA CTA GTC ATA TGT CTG CGA GTC AGG ATT CT 3') and IF41_Mus_low (5' GCG CGC TCG AGA ATG

AGG TCA GCA ACG TTG A 3') that contained the same restriction sites as described for LieIF4A. Cloning into pET22b was as described above. The construction of the other expression vectors for LieIF4A (1–403), LieIF4A RecA-like domain 1 (1–238; LieIF4A-D1) and LieIF4A RecA-like domain 2 (239–403; LieIF4A-D2) was as previously described [20, 25].

The His6-tagged recombinant proteins were expressed in the Rosetta *Escherichia coli* strain, and the proteins were purified as previously described [20, 23, 25]. In parallel, catalytically inactivated proteins (GAT mutation of motif I) were purified to test for contaminating ATPases; these proteins showed a background activity of only a few percent of the wildtype proteins. Protein concentrations were determined by the Bio-Rad Protein Dye assay using BSA as a standard. The purity and concentrations were verified by electrophoretically separating the proteins on a 12% polyacrylamide Laemmli gel (Bio-Rad Mini-Protean; Hercules, CA, USA) containing sodium dodecyl sulfate (SDS-PAGE), and the proteins were visualized by staining the gels with Coomassie Brilliant Blue R-250. Purified proteins were stored in 50% glycerol at -80 °C until needed.

2.3. ATPase assay

We used a colorimetric assay to measure the phosphate released during ATP hydrolysis based on Malachite green as previously described [20]. The reaction buffers contained 50 mM potassium acetate, 20 mM MES, pH 6, 2 mM dithiothreitol (DTT), 0.1 mg/mL BSA and various concentrations of whole yeast RNA (Type XI-C, Sigma-Aldrich). We added 5 mM magnesium acetate to the LieIF4A reactions and 1 mM to those with $eIF4AI_{Mus}$; mouse eIF4AI was inhibited by high Mg^{2+} concentrations while LieIF4A was optimally active at the higher concentration [20]. Reactions were started by adding ATP and then incubated at 37 °C for various times in 1.5 mL Eppendorf tubes. Then, 50 µL aliquots

were taken and pipetted into 96 well microtiter plates. Reactions were stopped by making the solutions ~60 mM in ethylenediaminetetraacetic acid (EDTA). Each reaction was done in 50 µL volumes. The absorption at 630 nm was converted to phosphate concentration by a reference curve generated from a dilution series of a known phosphate concentration (0.1 mM Pi standard; Innova Biosciences). Reaction velocities were determined by a linear regression fit of the phosphate generated against time. Only the initial, linear phases of the curves were used. Velocities were determined for at least three independent experiments for each reaction condition. Data were analyzed with Kaleidagraph (Synergy).

2.4. RNA helicase activity

RNA helicase assays were similar to those previously described [27]. In brief, we used a 45-nucleotide-long RNA (K06; 5′ GGG CUA GCA CCG UAA AGC AAG UUA AUU CAA AAC AAA ACA AAA GCU 3′) that was transcribed *in vitro* by T7 RNA polymerase off of a HindIII-linearized template using the MEGAshortscript kit (Ambion ThermoFisher Scientific, Waltham, MA, USA). The RNA products were separated by electrophoresis on a 8% PAGE gel containing 7 M urea, and the band corresponding to the desired product was eluted, extracted with phenol, extracted with chloroform-isoamyl alcohol (24:1) and ethanol precipitated as previously described [28]. The centrifuged and dried pellet was resuspended in 20 mM Tris-HCl, pH 7.5, 0.1 mM EDTA and stored at -20 °C until needed. A 13-nucleotide-long RNA oligonucleotide (Hyb13-RNA; 5' CUU UAC GGU GCU A 3'; Dharmacon/Thermo Scientific, Lafayette, CO, USA) that was complementary to K06 was labeled at the 5' end with γ-^{32}P-ATP (~3000 Ci/mmole; PerkinElmer, Waltham, MA, USA) and T4 polynucleotide kinase (New England Biolabs, Ipswich, MA, USA for 30 minutes at 37 °C, heat inactivated at 65 °C for 20 minutes, and stored at -20 °C until needed.

The duplex was made by incubating ^{32}P-Hyb13 RNA with K06 RNA at equimolar concentrations in a solution containing 50 μM of each RNA, 200 mM potassium acetate 20 mM Tris-HCl, pH 8.0 and 0.1 mM EDTA. Annealing was accomplished with a MyCycler PCR (Bio-Rad) by heating to 80 °C for 30 seconds, slow cooling to 50 °C and incubating for 30 minutes, slow cooling to 30 °C and incubating for another 30 minutes and finally slow cooling to 4 °C. The duplex was subsequently extracted with phenol, extracted with chloroform-isoamyl alcohol and ethanol precipitated. The centrifuged and dried pellet was resuspended in a buffer containing 200 mM potassium acetate, 20 mM Tris-HCl, pH 7.5 and 0.1 mM EDTA at a duplex concentration of ~8 μM. The solution was incubated at 37 °C for 1 hour to ensure the duplex was equilibrated. Duplexes were stored at -20 °C until needed. The duplex had a calculated Gibbs free energy of -18.8 kcal/mole (-78.7 J/mole) in 1 M NaCl at 37 °C, by using the published nearest-neighbor-free-energy values [29].

Assays were done under the same buffer conditions as those used for the ATPase experiments. Reactions typically contained 50 nM of the ^{32}P-duplex, 1 mM ATP and 1 μM of an 18-nucleotide-long DNA oligonucleotide that was complementary to Hyb13 (α-Hyb1; 5' CTA GCA CCG TAA AGC AAG 3'). The 20-fold excess of α-Hyb1 oligonucleotide trapped the released Hyb13 RNA during the reaction and prevented it from re-annealing on the K06 RNA. Various concentrations of proteins were tested but we typically used 200 to 250 nM LieIF4A and 1000 nM eIF4AI$_{Mus}$. The higher amount of eIF4AI$_{Mus}$ was needed to compensate for its weaker helicase activity and to facilitate comparisons. Reactions were carried out at 37 °C for various times, the products were separated by electrophoresis on a 15% polyacrylamide gel at 4 °C under nondenaturing conditions, and the corresponding bands were quantified with an imaging plate (Fujifilm BAS-IP MS 2025) and a Typhoon FLA9500 (GE Healthcare) phosphoimager. Data were analyzed with Optiquant (Packard) and Kaleidagraph software.

2.5. Molecular modeling, molecular dynamics, cavity analysis and docking simulations

We used two models of LieIF4A that corresponded to the ligand-free form ("open") and ligand-bound form ("closed") that were constructed and subjected to 2 ns molecular dynamics (MD) simulations as previously described [23]. We took 100 snapshots of their trajectories to perform an exhaustive search of the cavities using an in-house software based on Lee and Richards solvent accessible surface detection algorithm [30], called mkgridX [31]. The cavities for each snapshot structure were identified by clustering as previously described [23]. Individual cavities less than 12 $Å^3$, the volume of a water molecule, were discarded. Cavities from different snapshots were clustered by protein contact similarity to define sites, called P1, P2, etc. Likewise, cavities also were detected on solved crystal structures for the human/mouse ortholog eIF4AI (DDX2A; PDB 3EIQ, chain D), the T4 bacteriophage Gp32 protein (PDB 1GPC) and bovine serum albumin (PDB 3V03, chains A, B).

Molecular docking of 6-α-aminocholestanol was performed with AutoDock 4.2 [32], and we targeted all pockets identified on Gp32, DDX2A, BSA and on the 200 snapshots of both conformations of LieIF4A. PDBQT files of the ligand and the receptors were prepared using AutoDock Tools. One receptor file was generated per protein or snapshot by adding all the hydrogen atoms, adding the Gasteiger atomic charges, deleting nonpolar hydrogens and merging their charges with the carbon atoms, assigning atom types, detecting a root atom for the torsion tree and finally defining the rotatable bonds. The grid maps required by AutoDock were generated using AutoGrid [32] for each pocket by using the corresponding receptor file and by focusing on the geometrical center of the pocket defined by the ensemble of its residues. Point spacing was 0.375 Å. The Lamarckian Genetic algorithm of AutoDock 4 was used for the conformation search step, and it was coupled to a clustering analysis step.

The docking poses with the lowest docking scores on each cavity were retained. Poses with an estimated energy of binding higher than -6 kcal/mol were considered as nonsignificant [33]. For the retained docking poses, we generated the corresponding interaction diagrams using LigPlot+ with its default parameters [34]. Structures were visualized and manipulated with Swiss-PDBViewer 4.1.0 (http://www.expasy.org/spdbv/)[35]. Protein surfaces with the electrostatic potentials were done with the default settings.

3. Results

3.1. 6-aminocholestanol competitively inhibits the ATPase activity

We previously compared the ATPase activity of LieIF4A and $eIF4AI_{Mus}$ and found that 6-aminocholestanol inhibited both proteins to a similar extent [23]. In this work, we undertook more extensive kinetic analyses of the mode of inhibition on LieIF4A. DEAD-box proteins are RNA-dependent ATPases, so we determined the Michaelis–Menten parameters with saturating concentrations of RNA in the absence or presence of different quantities of 6-aminocholestanol (Fig. 1a). We obtained a K_m of 150 ± 20 μM (standard error of the regression) in the absence of the compound, which showed a higher binding affinity than what we previously measured (350 μM) [20]. Similarly, the k_{cat} (V_{max}/[LieIF4A]) was 2.4 ± 0.1 min^{-1}, which was 2-fold higher than our previously measured value. This probably reflected the different RNA substrates, protein preparations and particularly the presence of DMSO.

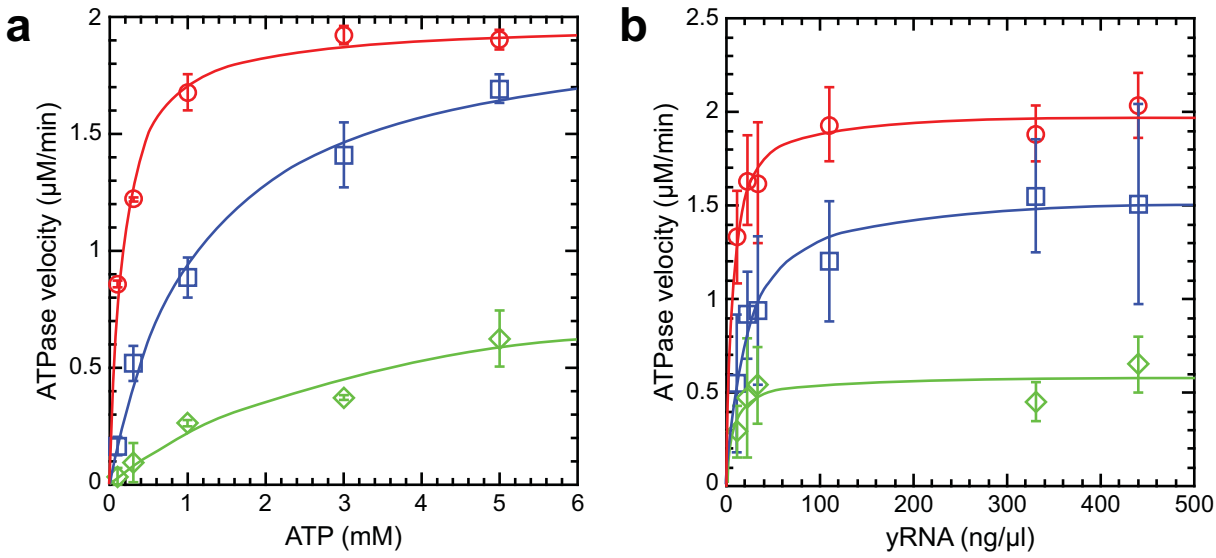

Fig. 1. ATPase reaction velocities of LieIF4A. The means and standard deviations are shown for three or more independent experiments. The values were fit to the nonlinear Michaelis–Menten equation $v = V_{max}[S]/(K_m + [S])$, where [S] is the substrate concentration, K_m is the Michaelis–Menten binding constant and V_{max} the maximum reaction velocity, using Kaleidagraph software. All the reactions were done in the presence of 10% DMSO and 820 nM LieIF4A. Red o, no added compound; blue □, 100 µM 6-aminocholestanol; green ◊, 300 µM 6-aminocholestanol. (a) The reaction velocities of LieIF4A with 340 ng/µl RNA and different concentrations of ATP, in the presence or absence of 6-aminocholestanol, are as indicated. (b) The reaction velocities of LieIF4A with 5 mM ATP at different concentrations of whole yeast RNA in the presence or absence of 6-aminocholestanol.

With the addition of 100 µM 6-aminocholestanol, the kinetic parameters were a K_m of 1100 ± 200 µM and a k_{cat} of 2.5 ± 0.2 min^{-1} (Fig. 1a). This was initially perplexing because the pronounced increase in the K_m for ATP indicated that the compound was reducing the affinity of LieIF4A for ATP rather than for RNA, which would have been expected to affect the k_{cat}. Similarly, with 300 µM 6-aminocholestanol we obtained a K_m of 3700 ± 2600 µM and a k_{cat} of 1.2 ± 0.4 min^{-1} (Fig 1a). This measured weak binding affinity for ATP was near the limit of sensitivity of our experimental assay, and consequently the values showed much higher uncertainty. Nevertheless, the values were again consistent with the compound primarily weakening ATP binding.

The Lineweaver–Burke plot was consistent with competitive inhibition of ATP binding. We subsequently fit our data to various formulations of the Dixon plot [36]. There was significant variability in the data but we obtained an inhibition constant, K_i, of around 35

to 100 μM, which indicated a higher binding affinity for 6-aminocholestanol than for ATP. Competitive inhibition was most consistent with the compound directly competing with ATP for the binding site on the protein rather than blocking the RNA. However, it was previously shown that ligands (RNA and ATP) show positive cooperative binding to $eIF4AI_{Mus}$ [37]. Consequently, it was possible that 6-aminocholestanol binding at the RNA site could alter the affinity of the protein for ATP and consequently allosterically affect ATP binding. This would be consistent with our molecular modeling studies that indicated that the binding site exists only in the open conformation of the RecA-like domains [23]. Thus, the compound might "lock" the protein in a conformation that had a low affinity for ligands.

3.2. 6-aminocholestanol competitively inhibits RNA binding

We initially tried electrophoretic mobility shift assays (EMSA)[38] with fluorescent-labeled RNA oligonucleotides (5' Cy5-UCA UAC UUU UCU UUU CUU UUC CAU C-3') to measure the effects of the compound on RNA binding. Unfortunately, the relatively weak RNA binding and high protein concentrations that were needed gave a weak signal that was not easy to interpret. Consequently, we used Michaelis–Menten kinetics to measure the effects of varying the concentration of whole yeast RNA under saturating ATP concentrations in the presence and absence of 6-aminocholestanol. There was experimental scatter, but the data showed a good fit to the nonlinear Michaelis–Menten equation (Fig 1b). Again, the compound primarily reduced the binding affinities (higher K_m) for RNA; the values for k_{cat} were 2.3 ± 0.1 min^{-1} in the absence of compound, 1.9 ± 0.1 min^{-1} with 100 μM 6-aminocholestanol and 0.71 ± 0.09 min^{-1} with 300 μM. The whole yeast RNA represented a heterogeneous mix of substrates, and consequently the actual concentration of the RNA substrates was unknown; thus we could only determine relative K_m values. We found that the K_m for the RNA was increased 3.6 ± 0.7–fold with 100 μM of the compound, which was

consistent with 6-aminocholestanol indirectly affecting ATP binding and catalysis by interfering with RNA binding, but the results were not conclusive.

3.3. 6-aminocholestanol binds to nucleic acid-binding proteins

In our initial modeling, molecular dynamics and docking simulations, 6-aminocholestanol bound in a pocket formed in the open conformation of the protein that consisted, in part, by RNA-interacting motifs Ia, GG and Ib, which are within RecA-like domain 1 [23]. If this were true, then domain 1 should bind the compound independently of the rest of the protein. We tested this by using the isolated RecA-like domain 1 as a competitor for compound binding in the ATPase assays. LieIF4A showed a reaction velocity of 1.89 μM/min in the presence of RNA and 10% DMSO, which we defined as a relative activity of 100% (Table 1). LieIF4A had ~8% of the ATPase activity in the absence of RNA (0.16/1.89). The RNA-dependent ATPase activity was reduced nearly 8-fold by the presence of 300 μM 6-aminocholestanol (1.89/0.24; Table 1).

Table 1. The RNA-dependent ATPase activity.

Protein[a]	RNA[b]	6-NH-cholestanol[c]	V (μM/min)[d]	Relative[e]
LieIF4A	+	–	1.89 ± 0.25	1.00 ± 0.13
LieIF4A	–	–	0.16 ± 0.02	0.08 ± 0.01
LieIF4A	+	+	0.24 ± 0.02	0.13 ± 0.01
LieIF4A + D1	+	–	2.28 ± 0.20	1.21 ± 0.10
LieIF4A + D1	+	+	1.67 ± 0.07	0.88 ± 0.04
LieIF4A + D1-GAT	+	–	1.34 ± 0.15	0.71 ± 0.08
LieIF4A + D1-GAT	+	+	1.29 ± 0.19	0.68 ± 0.10
LieIF4A + D2	+	–	1.60 ± 0.18	0.85 ± 0.10
LieIF4A + D2	+	+	1.08 ± 0.06	0.57 ± 0.03
LieIF4A + Gp32	+	–	1.99 ± 0.24*	1.05 ± 0.13*
LieIF4A + Gp32	+	+	1.63 ± 0.06	0.86 ± 0.03
LieIF4A + BSA	+	–	1.72 ± 0.13	0.91 ± 0.07
LieIF4A + BSA	+	+	0.24 ± 0.05*	0.13 ± 0.02*
D1	–	–	0.16 ± 0.04	0.08 ± 0.02
D1	–	+	0.27 ± 0.17	0.14 ± 0.09
D1	+	–	0.40 ± 0.17	0.21 ± 0.09
D1	+	+	0.20 ± 0.02	0.11 ± 0.01
D1-GAT	+	–	0.18 ± 0.09	0.10 ± 0.05
D2	+	–	0.03 ± 0.02	0.02 ± 0.01

[a] LieIF4A (1-403), 820 nM; D1, RecA-like domain 1 (1–238), 8.8 μM; D1-GAT, 8.7 μM; D2, RecA-like domain 2 (239–403), 7.9 μM; Gp32, 8.0 μM Bacteriophage T4 gene 32; BSA, 8.4 μM bovine serum albumin.
[b] Whole yeast RNA, type XI-C (Sigma-Aldrich), when present, was used at 340 ng/μl (~1 mM in mononucleotides). This was saturating for the ATPase activity.
[c] 6-aminocholestanol was dissolved in DMSO and used at 300 μM. Rows with the compound are shown shaded.
[d] Mean velocity of the ATPase activity from three or more independent experiments, unless otherwise noted. The Standard deviations around the mean are shown. All reactions were done in the presence of 10% DMSO. The ATP was used at 1 mM.
[e] The ATPase velocity relative to LieIF4A under optimal conditions. The standard deviations were calculated from the relative values.
*Only two independent measurements were made.

We then added a 10-fold molar excess of the purified RecA-like domain 1 (1–238 aa), which we predicted would sequester the compound, reduce its effective concentration and thereby partially restore the ATPase activity. Unexpectedly, RecA-like domain 1, by itself, increased the apparent ATPase activity of LieIF4A in the absence of the compound (2.28 versus 1.89; Table 1). This could have resulted from an activation of LieIF4A by RecA-like domain 1 or by an intrinsic ATPase activity of domain 1. Nevertheless, domain 1 was able to restore the ATPase activity of LieIF4A to ~73% (1.67/2.28; Table 1) of the uninhibited protein in the presence of 6-aminocholestanol, which was consistent with it binding and sequestering the compound.

DEAD-box proteins are considered RNA-dependent ATPases that hydrolyze the ATP in the closed configuration of the two RecA-like domains, which brings all the conserved motifs in close proximity [6, 7, 12]. Therefore, the "activation" by RecA-like domain 1 was surprising. We tested this by repeating the ATPase assays but with only domain 1 as a source of protein. It had ~8% (0.16/1.89) of the ATPase activity of LieIF4A in the absence of RNA and ~21% (0.40/1.89) in it presence; thus, the increased ATPase activity was entirely due to the intrinsic ATPase activity of domain 1 (Table 1). However, this result exaggerated the intrinsic activity because domain 1 was used at a ~10-fold molar excess over LieIF4A. Consequently, domain 1 had only ~2.1% of the ATPase activity of LieIF4A at equimolar

concentrations. Under these circumstances, the compound should inhibit the RNA-dependent ATPase activity of domain 1 as well, which was what we found. The activity was reduced to that of the level found in the absence of RNA (Table 1). This provided further evidence that 6-aminocholestanol was directly interfering with RNA binding, as expected from the molecular modeling.

It remained possible that domain 1 directly affected the activity of LieIF4A but that this effect was hidden by the intrinsic ATPase activity of domain 1. We tested this with a variant form of LieIF4A domain 1 (D1-GAT) that had a lysine 76 to alanine mutation in the phosphate binding loop (P-loop) of motif I. This mutation has no detectable RNA-dependent ATPase activity when made in the intact protein [20]. When added to LieIF4A, this mutated domain 1 reduced its activity by ~29% (1.34/1.89) in the absence of the compound (Table 1). However, the added compound had only a small additional effect (~4% less active; 1.29/1.34), which demonstrated that domain 1 was capable of efficiently sequestering the molecule. This was consistent with 6-aminocholestanol binding primarily to the open (ligand-free) conformation of LieIF4A, as predicted from the molecular modeling [23]. The full-length LieIF4A protein in the presence of ligands would be expected to be often in the closed conformation and hence less accessible to the compound. It was unclear why the GAT mutant of domain 1 by itself inhibited the ATPase activity of LieIF4A, but it was possible that it interfered with the formation of the catalytically active conformation of the protein. It might also reduce the effective concentration of the RNA available to LieIF4A even though we used a large excess of RNA.

Both RecA-like domains of DEAD-box proteins bind the RNA ligands. Our modeling predicted that the compound would bind primarily to domain 1 but it might also bind the RNA site on domain 2. We tested this by repeating the experiments with a 10-fold molar excess of the purified domain 2 (239–403 aa). Domain 2 by itself reduced the ATPase activity

of LieIF4A by ~15% (1.60/1.89), which was about half of what we obtained with the domain 1 GAT mutant (Table 1). However, 6-aminocholestanol further reduced the activity, relative to the wildtype activity (LieIF4A), by only an additional ~28% (85% less 57%). The net result was that the compound reduced the ATPase activity of LieIF4A with domain 2 (LieIF4A+D2) by only ~33% (57/85), which was much less than the nearly 8-fold inhibition we obtained in the absence of domain 2. Domain 2 had negligible intrinsic ATPase activity. Thus, the compound also was able to bind to RecA-like domain 2 but with a lower overall affinity.

It remained possible that 6-aminocholestanol was binding nonspecifically on multiple positions of the protein that were unrelated to the RNA binding site. We tested this by adding a 10-fold molar excess of bovine serum albumin (BSA), which has no known affinity for nucleic acids. BSA by itself reduced the ATPase activity of LieIF4A by ~9% (1.72/1.89; Table 1). However, it had no or only a slight affect on the inhibition by the compound. Thus, BSA was ineffective at binding the molecule. If 6-aminocholestanol specifically interfered with RNA binding, then it was possible that other nucleic acid-binding proteins would sequester the compound and reduce the inhibition of the RNA-dependent ATPase activity of LieIF4A. We tested this by adding a 10-fold molar excess of bacteriophage T4 gene 32 (Gp32), which is known to bind both single-stranded DNA and RNA, although the latter with much less affinity [39]. The Gp32 protein by itself had negligible affect on the ATPase activity of LieIF4A (Table 1). This result, plus the result with BSA, indicated that the more pronounced inhibition with the individual RecA-like domains, in the absence of the compound, was the result of more specific interactions between the separate domains and LieIF4A. In contrast, the ATPase activity of LieIF4A in the presence of 300 μM 6-aminocholestanol was reduced by only ~18% (1.63/1.99) with a 10-fold molar excess of Gp32. Thus, Gp32 was nearly 50% more effective than domain 2 at sequestering the

compound, but it was only ~85% (82%/96%) as effective as the domain 1 GAT mutant. This meant that the RecA-like domain 1 had a higher affinity for the molecule, which was consistent with it interacting primarily at the site we identified by molecular modeling [23].

3.4. 6-aminocholestanol inhibits the helicase activity

The preceding experiments showed that 6-aminocholestanol inhibited the ATPase activity of LieIF4A by interfering with RNA and perhaps ATP binding. Therefore, it was likely that the compound would inhibit the helicase activity of LieIF4A as well. We previously showed that, like most DEAD-box proteins, LieIF4A was capable of displacing short duplexes that were either 5' or 3' to single-stranded regions; the single-stranded RNA functioned as loading sites that greatly enhance the enzymatic activity [20]. We used a variant of the previous system that consisted of a 13-nucleotide-long RNA oligonucleotide, which was labeled on the 5' end with ^{32}P, hybridized to a 45-nucleotide-long RNA template (Fig. 2a). This duplex was stable under the reaction conditions (Fig. 2c), and it would reform if disrupted. Consequently, we added a 20-fold excess of a DNA oligonucleotide "trap" that was complementary to the released ^{32}P-labeled RNA oligonucleotide (Fig. 2b). The resulting DNA-RNA duplex migrated as smaller product during electrophoresis on a nondenaturing polyacrylamide gel (Fig. 2c).

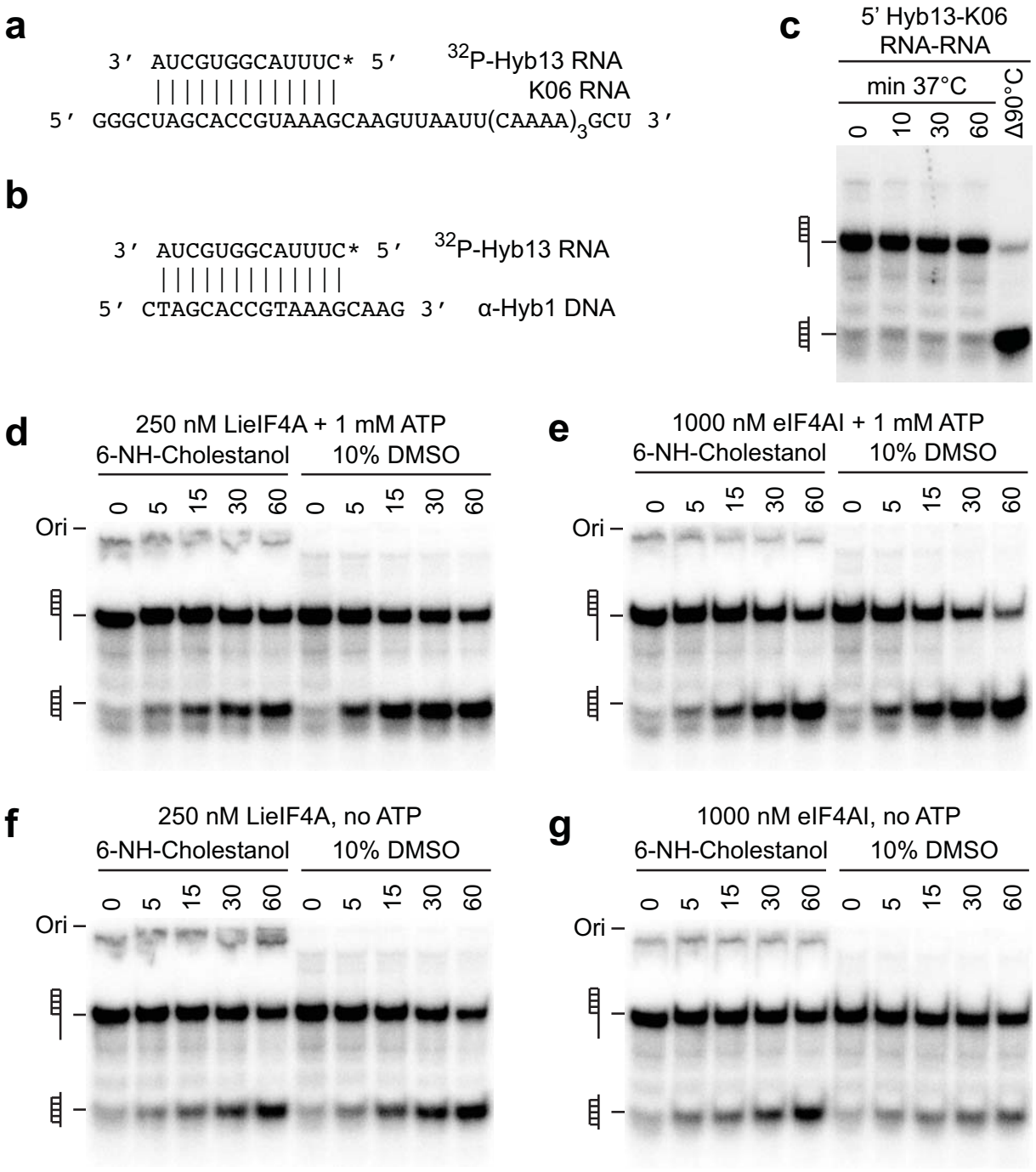

Fig. 2. The helicase activity of LieIF4A. (a) The helicase substrate was made by hybridizing a 13-nucleotide-long RNA (Hyb13) that was labeled on the 5' end with ^{32}P (*) with a 45-nucleotide-long template RNA (K06) that was not labeled. (b) The Hyb13 released during the helicase reaction was "trapped" by a complementary DNA oligonucleotide (α-Hyb1) that was presence at 20-fold excess of Hyb13. (c) The duplex was stable under the reaction conditions in the absence of LieIF4A. However, samples heated to 90 °C formed ≥95% of the Hyb13-α-Hyb1 duplex that migrated faster then the Hyb13-K06 duplex on a 15%, nondenaturing, polyacrymide gel run at 4 °C. (d) LieIF4A at 250 nM unwinds 50 nM of the duplex in the presence of 1 mM ATP in a time-dependent fashion (shown in minutes). All reactions were done in the presence of 10% DMSO. Ori, indicates the position of the bottom of the wells. In the presence of 100 μM 6-aminocholestanol, a small amount of ^{32}P-Hyb13, or a complex thereof, migrated as a much higher molecular weight species. (e) An equivalent unwinding

assay as (d) but with 1000 nM eIF4AI$_{Mus}$. (f) The same experiment as that shown in (d) but without added ATP. (g) The same experiment as that shown in (e) but without added ATP.

We carefully calibrated the concentrations of LieIF4A and eIF4AI$_{Mus}$ to give comparable unwinding activities over the time course of the reaction in the presence of 1 mM ATP and 10% DMSO. We found that 250 nM of LieIF4A and 1000 nM of eIF4AI$_{Mus}$ gave the best results (Fig. 2d and 2e). We initially tried 300 μM 6-aminocholestanol, but we were unable to detect any resulting helicase activity. Consequently, we did all the subsequent experiments with 100 μM of the compound. The compound inhibited the helicase activity of both LieIF4A and eIF4AI$_{Mus}$ but to somewhat different extents (Figs 2d and 2e). Moreover, the 6-aminocholestanol caused a small amount of ^{32}P-Hyb13, or a complex thereof, to migrate as a much higher molecular weight species. We added ~0.3% SDS to the loading buffer to block protein-RNA interactions, but either the ^{32}P-Hyb13 interactions with the protein were stabilized by the compound or the molecule promoted aggregation of the nucleic acids. We quantified the bands with a phosphoimager and plotted the percentage of the duplex unwound with time.

LieIF4A and eIF4AI$_{Mus}$ had different reaction profiles (Fig 3a). In the absence of 6-aminocholestanol, LieIF4A showed a faster initial rate than eIF4AI$_{Mus}$ but it tended to plateau with less duplex unwound. LieIF4A was used at a 4-fold lower concentration, which would partially explain why eIF4AI$_{Mus}$ showed a plateau with more duplex unwound. It also was possible that LieIF4A was losing enzymatic activity more rapidly than eIF4AI$_{Mus}$ during the course of the reaction. The 6-aminocholestanol inhibited the helicase activity of both proteins. Comparisons were difficult because only the initial phase of the curves could be used, which contained limited data. Nevertheless, the compound reduced the helicase reaction velocities of LieIF4A by 3.3- to 5.6-fold and of eIF4AI$_{Mus}$ by 2.6- to 3.4-fold.

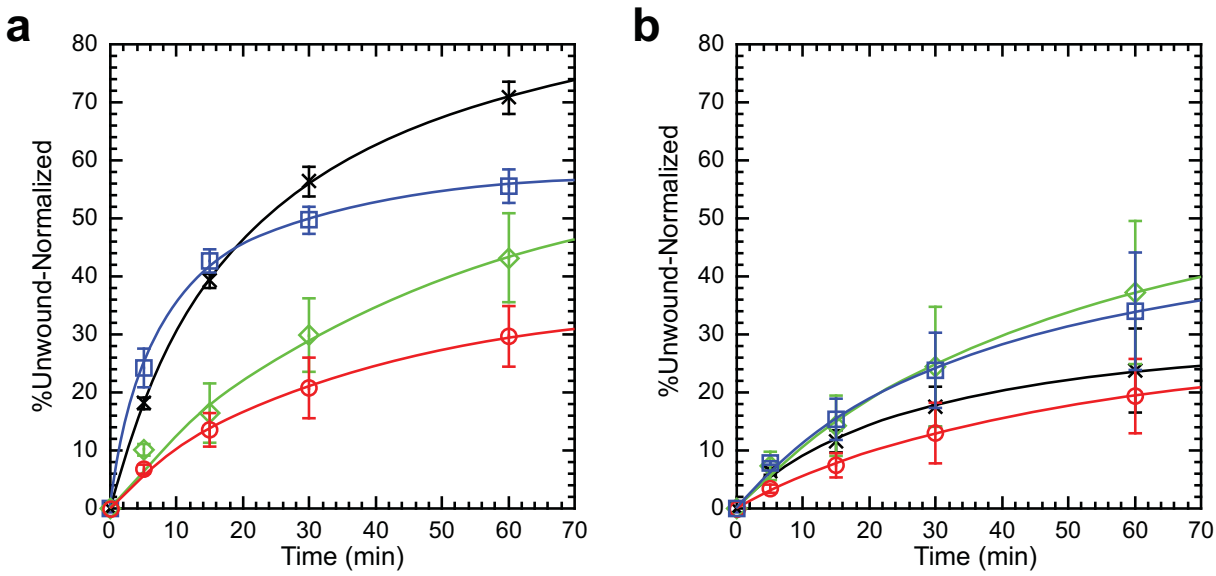

Fig. 3. Normalized mean unwinding activity of LieIF4A and eIF4AI$_{Mus}$. All reactions were done in the presence of 10% DMSO. The mean and standard deviations are shown for three or more independent experiments. Blue □, LieIF4A; red o, LieIF4A with 100 µM 6-aminocholestanol; black x, eIF4AI$_{Mus}$; green ◊, eIF4AI$_{Mus}$ with 100 µM 6-aminocholestanol. (a) The unwinding activities in the presence of 1 mM ATP. (b) The unwinding activities in the absence of ATP.

We typically do parallel experiments in the absence of ATP because the high protein concentrations cause ATP-independent unwinding, probably through a mass-action effect. Indeed, we saw significant unwinding even in the absence of ATP for both LieIF4A and eIF4AI$_{Mus}$ (Fig. 2f and 2g). Oddly, while added 6-aminocholestanol reduced this activity for LieIF4A, it actually increased the activity for eIF4AI$_{Mus}$ in the absence of ATP. We quantified the bands with a phosphoimager and plotted the percentage of unwinding in Figure 3b. The compound reduced the activity of LieIF4A by 44% and increased the activity of eIF4AI$_{Mus}$ by 43% in an ATP-independent manner. The net result was that eIF4AI$_{Mus}$ in the presence of 6-aminocholestanol had as much helicase activity as LieIF4A in the absence of the compound, although the latter protein was 4-fold less concentrated. It was possible that the compound stabilized protein-RNA interactions that promoted the ATP-independent unwinding of eIF4AI$_{Mus}$. This would not be true for LieIF4A because our modeling studies indicated that the primary binding sites existed in the open complex that would lack helicase activity. Thus,

LieIF4A and eIF4AI$_{Mus}$ appear to have different binding sites and to behave differently to the presence of the compound.

As noted above, it was possible that the DMSO used to solubilize the compounds affected the enzymatic properties of the proteins. This would account for why the Michaelis-Menten values we obtained for the RNA-dependent ATPase assays showed 2-fold higher binding affinities and ATP hydrolysis rates for LieIF4A than previously determined [20]. We repeated the helicase experiments of LieIF4A and eIF4IA$_{Mus}$ with the K06-Hyb13 RNA duplex in the presence of 1 mM ATP and the presence or absence of 10% DMSO (Supplementary data Fig. S1) and quantified the results in Figure 4. We found that the DMSO significantly enhanced the unwinding reaction of both LieIF4A and eIF4AI$_{Mus}$, but that the increased activity was more pronounced for LieIF4A. DMSO is a polar aprotic solvent that is capable of dissolving both polar and nonpolar compounds [40]. It may have destabilized the RNA duplex, but DMSO is also known to enhance the flexibility of proteins and to enhance or inhibit enzymatic activities [40-43].

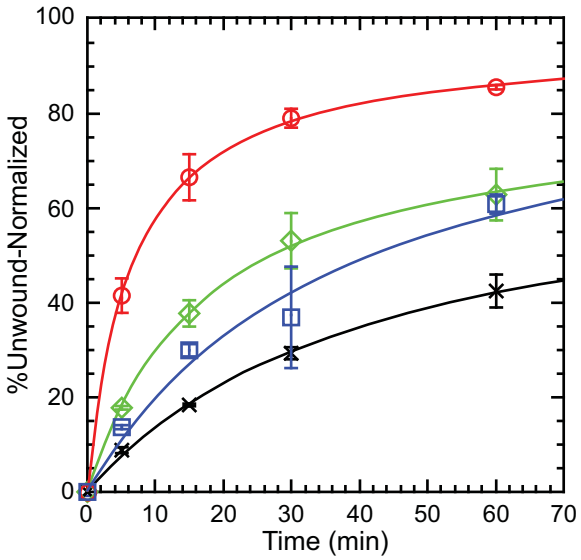

Fig. 4. Normalized mean unwinding activity of LieIF4A and eIF4AI$_{Mus}$ ±10% DMSO. Reactions were done in the presence or absence of 10% DMSO and 1 mM ATP. The mean and standard deviations are shown for three or more independent experiments. Blue □, LieIF4A; red o, LieIF4A with 10% DMSO; black x, eIF4AI$_{Mus}$; green ◊, eIF4AI$_{Mus}$ with 10% DMSO.

3.5. Molecular modeling, dynamics and docking simulations

The experimental results we obtained indicated that there were additional binding sites on LieIF4A that were not previously taken into account [23]. Therefore, we re-analyzed our molecular dynamics through an exhaustive search for cavities and pockets on the protein surface in its open and closed conformations, and we re-performed docking simulations of 6-α-aminocholestanol on the identified pockets. We undertook similar analyses on the solved crystal structure of $eIF4AI_{Mus}$, and as controls on the solved crystal structures of Gp32 and BSA.

The identified cavities were then examined for their potential to be effective binding sites for 6-α-aminocholestanol. A total of 60 cavities were identified that mostly appeared either on the open or closed forms of LieIF4A, but eleven of these pockets were detected on both states. We further investigated the distribution of the docking scores obtained on LieIF4A for each of the 60 pockets. Only eighteen out of the 60 pockets demonstrated at least one binding mode of the compound with a negative docking score, and they were retained for further analyses. Of these eighteen, only five demonstrated significant docking scores of -6 kcal/mole or less (Table 2) [33]. Three of these pockets (P11, P19, P29; Fig. 5a–5c) were found only on the open conformation and two (P26, P39; Fig. 5d, 5e) were only on the closed form. The pockets P19, P26, P29 and P39 were in the interdomain cleft between the two RecA-like domains while P11 was in the previously identified pocket in domain 1 [23]. The docked compounds in all the identified pockets made significant interactions with the conserved motifs involved in ligand binding, and many of these interactions were overlapping in the different pockets (Fig. 5, 6).

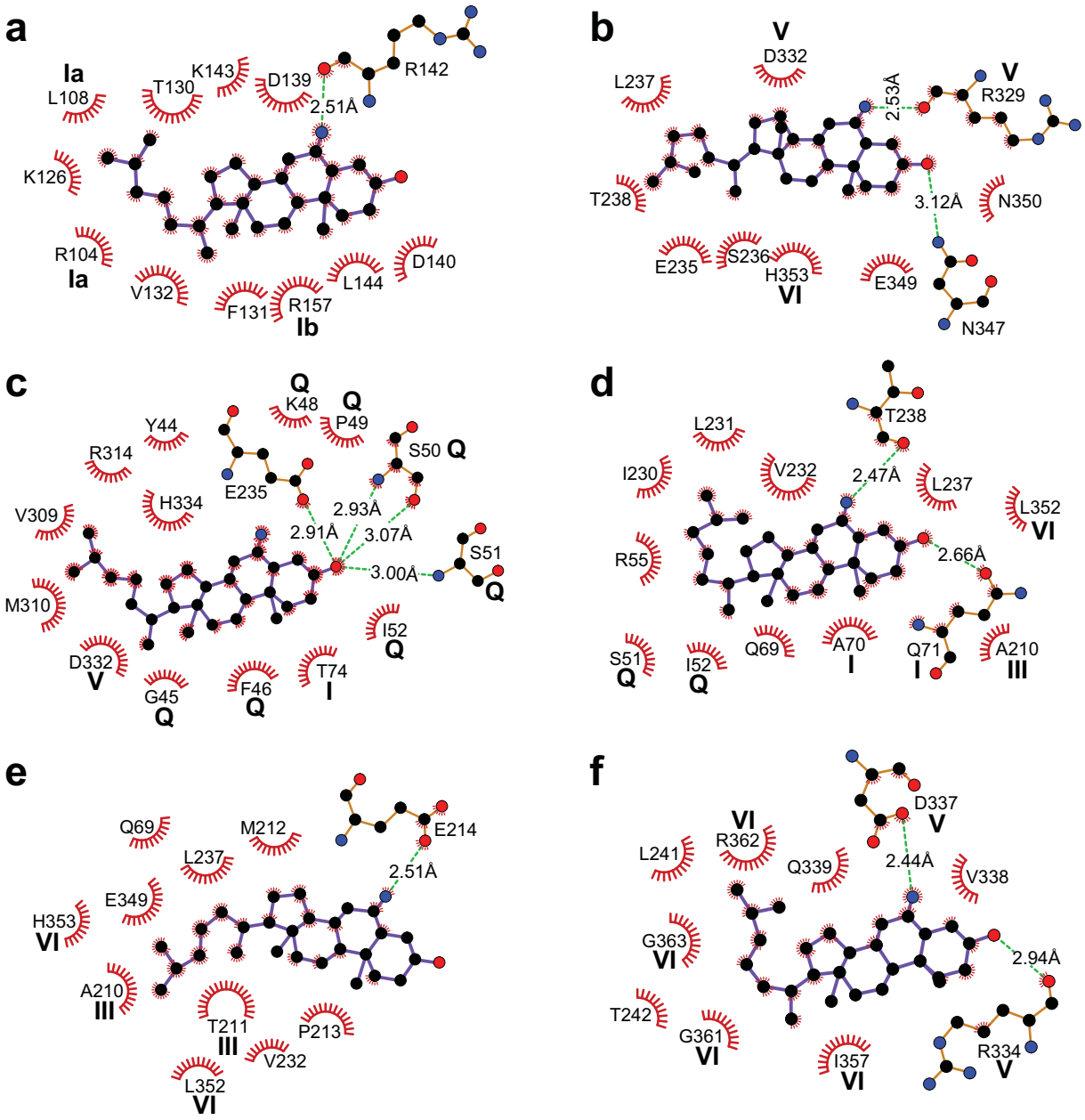

Fig. 5. Interactions of 6-α-aminocholestanol on the identified pockets of LieIF4A and eIF4AI$_{Mus}$ as determined with LigPlot+. Interactions involving residues in conserved motifs are as indicated. The red "brushes" represent van der Waals force interactions and the dotted green lines represent hydrogen bonds. (a) The compound bound in pocket P11 of the open form of LieIF4A. (b) The compound in pocket P19 of the open form of LieIF4A. (c) The compound in pocket P29 of the open form of LieIF4A. (d) The compound bound in pocket P26 of the closed form of LieIF4A. (e) The compound in pocket P39 of the closed form of LieIF4A. (f) The compound in pocket P14 of the open form of eIF4AI$_{Mus}$.

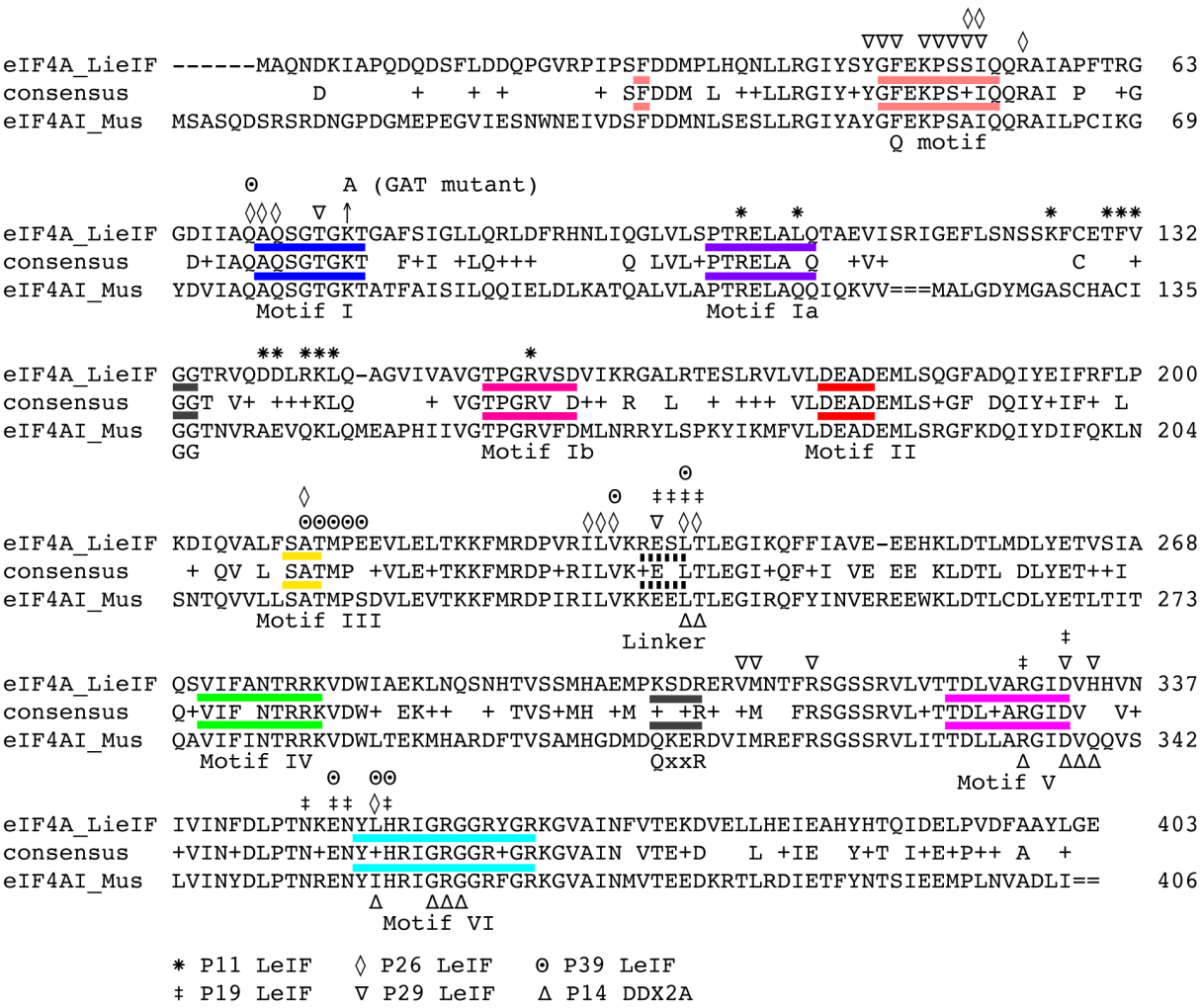

Fig. 6. Location of the interactions of 6-α-aminocholestanol on LieIF4A and eIF4AI$_{Mus}$. The linker region between RecA-like domain 1 and domain 2 is indicated with a dotted line. Interactions of P11 LieIF4A, P19 LieIF4A, P26 LieIF4A and P14 DDX2A (eIF4AI$_{Mus}$) involve the "open" conformation. Interactions of P29 LieIF4A and P39 LieIF4A involve the "closed" conformation. The position of the LieIF4A GAT mutation of domain 1 is as shown.

We conducted similar cavity search and docking simulations on the mammalian ortholog eIF4AI (DDX2A), and we obtained results that indicated a unique potential binding site with a significant binding energy (P14; Fig. 5f, Fig. 6; Table 2). It was well below the cutoff value of -6 kcal/mole. Pocket P14 was located in the central part of the inter-domain cleft. The interactions of its amino acids overlapped with those of the four pockets of the inter-domain cleft of LieIF4A (Fig. 5, 6). The docking score for eIF4AI P14 was comparable to those obtained for the LieIF4A pockets (Table 2).

Table 2. Docking scores and positions of 6-α-aminocholestanol on proteins.

Protein	Form	Pocket	Score[a]	Interact.[b]	%D1[c]	%Link.[c]	%D2[c]
LieIF4A	open	P11	-9.16	12	100	0	0
LieIF4A	open	P19	-6.35	10	0	30	70
LieIF4A	open	P29	-10.14	15	60	6.7	33.3
LieIF4A	closed	P26	-9.04	13	76.9	7.7	15.4
LieIF4A	closed	P39	-9.58	11	63.6	9.1	27.3
DDX2A	open	P14	-9.19	10	0	10	90
Gp32	NA[d]	P17	-4.47	10	NA	NA	NA
BSA	NA	P12	-10.7	11	NA	NA	NA
BSA	NA	P18	-8.24	16	NA	NA	NA
BSA	NA	P32	-8.22	12	NA	NA	NA
BSA	NA	P42	-7.56	15	NA	NA	NA

[a] The scores represent the calculated binding energies in kcal/mole.
[b] The interactions represent the number of amino acids that form hydrogen bonds and van der Waals force interactions with the compound.
[c] The fraction of interactions that occur in RecA-like domain 1, RecA-like domain 2 or in the linker region between the two domains.
[d] Not applicable.

As a control, we made cavity search and simulations on the solved crystal structures of bacteriophage T4 Gp32 and BSA. The former was an effective competitor for the compound while the latter was not. We obtained a single binding site on Gp32 with negative binding energy that was located on the putative nucleic acids binding site, but it was significantly above the cutoff value of -6 kcal/mole (P14; Supplementary data Fig. S2, Table 2). However, the solved crystal structure was missing 27.6% of its amino acids; consequently there may have been other sites on the full-length protein that were not detected by our molecular simulations. Moreover, the missing amino terminus was close to the binding site, and it might have enhanced the affinity for the compound. Hence, proteins with nucleic acids binding sites are potential targets for the compound, and therefore it is important to take into consideration such off-target effects in screening for more specific inhibitors.

In contrast, we found four binding pockets on BSA with binding energies that were well below the cutoff of -6 kcal/mole (Table 2). We used both chains of the solved crystal structure but only one (P32) of the four pockets was found on both chains. Notably, P32 made no specific hydrogen bonds with the ligand. Chain B was missing A583 and A584, and both

chains lacked the first 26 amino-terminal residues. Both chains were largely superimposable, and the missing amino-acid residues were far from the identified binding pockets. This suggests that there were subtle differences in the structures, and that the pockets identified might not be representative of those found in solution. Moreover, the DMSO in the solution may have more profound affects on the conformation of BSA than for the other proteins. Indeed, it is known that BSA becomes partially denatured in DMSO [44].

4. Discussion

Trypanosomatids and many fungi have an essential requirement for ergosterol, which is a 24-alkyl sterol that serves a similar role to cholesterol in membrane fluidity; it is not utilized in animals [45, 46]. As a consequence, the biosynthetic pathway of ergosterol is a common target for antifungal and anti-protozoan drugs [47, 48]. Among these candidate drugs are the epimers 6-α/ß-aminocholestanol and the related 7-α/ß-aminocholestanol that target the $\Delta^8 \rightarrow \Delta^7$-sterol isomerase [24, 49]. However, we independently found through molecular modeling, molecular dynamics and docking simulations that 6-aminocholestanol could target the *L. infantum* LieIF4A protein, which is a probable ortholog of the translation-initiation factor eIF4A [20, 23]. Moreover, it shows structural similarity to the previously characterized hippuristanol that is an allosteric inhibitor of RNA binding in eukaryotic eIF4A-like proteins that locks the RecA-like domains in a nonproductive closed conformation [19].

We find that 6-aminocholestanol competitively inhibits both ATP and RNA binding to LieIF4A, and by doing so it inhibits the helicase activity of the protein as well. Our molecular dynamics, cavity analysis and docking simulations and competition assays with the individual RecA-like domains indicate that there are multiple binding sites for the compound on LieIF4A. Moreover, all of the identified binding pockets involve interactions with the

conserved motifs needed for ligand binding and enzymatic activities. With the exception of pocket P19, these interactions involve residues that are predominately located on RecA-like domain 1 (Table 2, Fig. 5, 6). However, only pocket P11 in the open conformation is found exclusively on domain 1, and this appears to be the primary binding site of the compound. Although not unique, the preferential binding of 6-aminocholestanol at this site demonstrates a degree of specificity in the binding.

In contrast, pocket P19 was exclusively on RecA-like domain 2 and the linker region between domains. It has a relatively weak docking score (Table 2) and the domain 2 fragment used in the competition experiments is missing the linker region; nevertheless, the D2 fragment is about 70% as effective as D1-GAT in sequestering the 6-aminochloestanol (after normalizing for the inhibitory effects of the isolated domains by themselves; Table 2). Hence, molecular dynamics and docking simulations correctly pointed to the existence of multiple plausible binding sites for the compound. Nevertheless, the docking scores we obtained are not closely representative of the actual binding affinities. This is not uncommon for docking on modeled structures. Moreover, our molecular dynamics simulations did not take into the account the effects of DMSO, which probably increased the protein flexibility.

The best docking score obtained is with pocket P29 in the open conformation. It makes extensive interactions with the Q motif, which is important for adenine recognition [50]. However, this pocket lacked the interactions with the critical 6-position amino group, which conferred ~11-fold higher inhibition than the equivalent compound with 6-position keto [23]. Consequently, it may have played a secondary role in the inhibitory effects of the compound. Likewise, it is unclear from our experiments what role(s) pockets P26 and P39 may play in the closed conformation (Fig. 5d, 5e). However, it should be noted that many of the pockets involve interactions with the same amino acids (Fig. 6).

Our cavity analysis and docking simulations revealed only a single binding pocket on the open conformation of eIF4AI$_{Mus}$, which was based on the solved crystal structure (Fig. 5f). Molecular modeling, molecular dynamics and docking simulations of the closed conformation might reveal additional sites. Nevertheless, the binding site we found is similar to that proposed for the allosteric inhibitor hippuristanol, which is thought to lock the RecA-like domains into an altered closed conformation [19]. We find that 6-aminocholestanol significantly enhances the ATP-independent unwinding activity of eIF4AI$_{Mus}$, which suggests that it too can lock the protein in an aberrantly closed conformation. Although hippuristanol and 6-aminocholestanol are both hydroxycholestanol derivatives, there are significant differences in their structures. Thus, in the future it may be useful to screen from a wide variety of hydroxycholestanol derivatives to select for those most specific for the eIF4A protein of the organism of interest.

The 6-aminocholestanol epimers were previously identified as antifungal agents because they could interfere with ergosterol biosynthesis [24]. Here, we find that they bind to and inhibit DEAD-box proteins as well. Nevertheless, these compounds interact with proteins in different ways and with different affects on their enzymology in accordance with previous results [23]. We demonstrated that they differently affect the mammalian and *Leishmania* proteins due to their different binding sites and affinities. Moreover, we note the occurrence of multiple compound-binding sites with major one(s) on LieIF4A RecA-like domain 1. We find it encouraging that the observation that 6-aminocholestanol binds certain sites with a higher affinity than others demonstrates a degree of specificity that can potentially be optimized by modifying the functionalities on the chemical backbone of the hydroxycholestanol. This will be facilitated once we have a solved crystal structure of LieIF4A with the bound compound, which is work currently in progress. Therefore, it is possible to screen for derivatives of these agents that selectively target DEAD-box proteins

from different organisms even when implicated in the same biological process. We hope that this work will foster further research in this domain.

Conflict of interest

The authors have no conflicts of interest to declare.

Acknowledgments

We thank Patrick Linder, Centre Médical Universitaire, Geneva, Switzerland, for the eIF4AI$_{Mus}$ clone. The 6-aminocholestanol was a gift from Dr. Leila el Kihel, Centre d'Etudes et de Recherche sur le Médicament de Normandie (CERMN), UFR des Sciences Pharmaceutiques, Université de Caen de Basse-Normandie, France, for the minimal costs of shipping fees. We thank Damien Monet for his assistance in the cavity generation and analyses. This work was supported by the Centre National de la Recherche Scientifique, by the HelicaRN [2010 BLAN 1503 01] and HeliDEAD grants [ANR-13-BSV8-0009-01] from the Agence Nationale de la Recherche, and by the Initiative d'Excellence program from the French State [Grant DYNAMO, ANR-11-LABX-0011-01] to NKT. This work received financial support from the Pasteur Institute Transversal Research Program (grant PTR426), and partially from the Ministry of Higher Education and Research in Tunisia (LR11IPT04 & LR16IPT04) to IG. EHS received support from the UNESCO-L'Oréal, "For Women in Science," international fellowship and the Institut Pasteur International Network (Calmette and Yersin programme).

References

[1] J. Alvar, I.D. Velez, C. Bern, M. Herrero, P. Desjeux, J. Cano, J. Jannin, M. den Boer, Leishmaniasis worldwide and global estimates of its incidence, PLoS One 7(5) (2012) e35671. https://doi.org/10.1371/journal.pone.0035671.

[2] N. Singh, B.B. Mishra, S. Bajpai, R.K. Singh, V.K. Tiwari, Natural product based leads to fight against leishmaniasis, Bioorg. Med. Chem. 22(1) (2014) 18-45. https://doi.org/10.1016/j.bmc.2013.11.048.

[3] S. Burza, S.L. Croft, M. Boelaert, Leishmaniasis, Lancet 392(10151) (2018) 951-970. https://doi.org/10.1016/s0140-6736(18)31204-2.

[4] M.S. Duthie, V.S. Raman, F.M. Piazza, S.G. Reed, The development and clinical evaluation of second-generation leishmaniasis vaccines, Vaccine 30(2) (2012) 134-141. https://doi.org/10.1016/j.vaccine.2011.11.005.

[5] O. Cordin, J. Banroques, N.K. Tanner, P. Linder, The DEAD-box protein family of RNA helicases, Gene 367 (2006) 17-37. https://doi.org/10.1016/j.gene.2005.10.019.

[6] P. Linder, E. Jankowsky, From unwinding to clamping - the DEAD box RNA helicase family, Nat. Rev. Mol. Cell. Biol. 12(8) (2011) 505-516. https://doi.org/10.1038/nrm3154.

[7] N.K. Tanner, P. Linder, DExD/H box RNA helicases: from generic motors to specific dissociation functions, Mol. Cell 8(2) (2001) 251-262.

[8] M. Senissar, A. Le Saux, N. Belgareh-Touze, C. Adam, J. Banroques, N.K. Tanner, The DEAD-box helicase Ded1 from yeast is an mRNP cap-associated protein that shuttles between the cytoplasm and nucleus, Nucleic Acids Res. 42(15) (2014) 10005-10022. https://doi.org/10.1093/nar/gku584.

[9] J. de la Cruz, D. Kressler, P. Linder, Unwinding RNA in *Saccharomyces cerevisiae*: DEAD-box proteins and related families, Trends Biochem. Sci. 24(5) (1999) 192-198.

[10] M. Abdelhaleem, L. Maltais, H. Wain, The human DDX and DHX gene families of putative RNA helicases, Genomics 81(6) (2003) 618-622.

[11] P.R. Gargantini, H.D. Lujan, C.A. Pereira, *In silico* analysis of trypanosomatids' helicases, FEMS Microbiol. Lett. 335(2) (2012) 123-129. https://doi.org/10.1111/j.1574-6968.2012.02644.x.

[12] P. Schutz, T. Karlberg, S. van den Berg, R. Collins, L. Lehtio, M. Hogbom, L. Holmberg-Schiavone, W. Tempel, H.W. Park, M. Hammarstrom, M. Moche, A.G. Thorsell, H. Schuler, Comparative structural analysis of human DEAD-box RNA helicases, PLoS One 5(9) (2010). https://doi.org/10.1371/journal.pone.0012791.

[13] L.A. Marchat, S.I. Arzola-Rodriguez, O. Hernandez-de la Cruz, I. Lopez-Rosas, C. Lopez-Camarillo, DEAD/DExH-Box RNA Helicases in Selected Human Parasites, Korean J. Parasitol. 53(5) (2015) 583-595. https://doi.org/10.3347/kjp.2015.53.5.583.

[14] W.R. Shadrick, J. Ndjomou, R. Kolli, S. Mukherjee, A.M. Hanson, D.N. Frick, Discovering new medicines targeting helicases: challenges and recent progress, J. Biomol. Screen. 18(7) (2013) 761-781. https://doi.org/10.1177/1087057113482586.

[15] R. Cencic, J. Pelletier, Throwing a monkey wrench in the motor: targeting DExH/D box proteins with small molecule inhibitors, Biochim. Biophys. Acta 1829(8) (2013) 894-903. https://doi.org/10.1016/j.bbagrm.2013.01.008.

[16] L. Steimer, D. Klostermeier, RNA helicases in infection and disease, RNA Biol. 9(6) (2012) 751-771. https://doi.org/10.4161/rna.20090.

[17] J. Chu, J. Pelletier, Targeting the eIF4A RNA helicase as an anti-neoplastic approach, Biochim. Biophys. Acta 1849(7) (2015) 781-791. https://doi.org/10.1016/j.bbagrm.2014.09.006.

[18] C.H. Chao, L.F. Huang, Y.L. Yang, J.H. Su, G.H. Wang, M.Y. Chiang, Y.C. Wu, C.F. Dai, J.H. Sheu, Polyoxygenated steroids from the gorgonian I*sis hippuris*, J. Nat. Prod. 68(6) (2005) 880-885. https://doi.org/10.1021/np050033y.

[19] R. Cencic, J. Pelletier, Hippuristanol - A potent steroid inhibitor of eukaryotic initiation factor 4A, Translation (Austin) 4(1) (2016) e1137381. https://doi.org/10.1080/21690731.2015.1137381.

[20] M. Barhoumi, N.K. Tanner, J. Banroques, P. Linder, I. Guizani, *Leishmania infantum* LeIF protein is an ATP-dependent RNA helicase and an eIF4A-like factor that inhibits translation in yeast, FEBS J. 273(22) (2006) 5086-5100. https://doi.org/10.1111/j.1742-4658.2006.05506.x.

[21] R. Dhalia, N. Marinsek, C.R. Reis, R. Katz, J.R. Muniz, N. Standart, M. Carrington, O.P. de Melo Neto, The two eIF4A helicases in *Trypanosoma brucei* are functionally distinct, Nucleic Acids Res. 34(9) (2006) 2495-2507. https://doi.org/10.1093/nar/gkl290.

[22] R. Dhalia, C.R. Reis, E.R. Freire, P.O. Rocha, R. Katz, J.R. Muniz, N. Standart, O.P. de Melo Neto, Translation initiation in *Leishmania major*: characterisation of multiple eIF4F subunit homologues, Mol. Biochem. Parasitol. 140(1) (2005) 23-41. https://doi.org/10.1016/j.molbiopara.2004.12.001.

[23] E. Harigua-Souiai, Y.Z. Abdelkrim, I. Bassoumi-Jamoussi, O. Zakraoui, G. Bouvier, K. Essafi-Benkhadir, J. Banroques, N. Desdouits, H. Munier-Lehmann, M. Barhoumi, N.K. Tanner, M. Nilges, A. Blondel, I. Guizani, Identification of novel leishmanicidal molecules by virtual and biochemical screenings targeting *Leishmania* eukaryotic initiation factor 4A, PLoS Negl. Trop. Dis. 12(1) (2018) e0006160. https://doi.org/10.1371/journal.pntd.0006160.

[24] P. Beuchet, L. el Kihel, M. Dherbomez, G. Charles, Y. Letourneux, Synthesis of 6(alpha, beta)-aminocholestanols as ergosterol biosynthesis inhibitors, Bioorg. Med. Chem. Lett. 8(24) (1998) 3627-3630.

[25] M. Barhoumi, A. Garnaoui, B. Kaabi, N.K. Tanner, I. Guizani, *Leishmania infantum* LeIF and its recombinant polypeptides modulate interleukin IL-12p70, IL-10 and tumour necrosis factor-alpha production by human monocytes, Parasite Immunol. 33(10) (2011) 583-588. https://doi.org/10.1111/j.1365-3024.2011.01320.x.

[26] A. Prat, S.R. Schmid, P. Buser, S. Blum, H. Trachsel, P.J. Nielsen, P. Linder, Expression of translation initiation factor 4A from yeast and mouse in *Saccharomyces cerevisiae*, Biochim. Biophys. Acta 1050(1-3) (1990) 140-145.

[27] J. Banroques, M. Doere, M. Dreyfus, P. Linder, N.K. Tanner, Motif III in superfamily 2 "helicases" helps convert the binding energy of ATP into a high-affinity RNA binding

site in the yeast DEAD-box protein Ded1, J. Mol. Biol. 396(4) (2010) 949-966. https://doi.org/10.1016/j.jmb.2009.12.025.

[28] O. Cordin, N.K. Tanner, M. Doere, P. Linder, J. Banroques, The newly discovered Q motif of DEAD-box RNA helicases regulates RNA-binding and helicase activity, EMBO J. 23(13) (2004) 2478-2487. https://doi.org/10.1038/sj.emboj.7600272.

[29] D.H. Turner, N. Sugimoto, S.M. Freier, RNA structure prediction, Annu. Rev. Biophys. Biophys. Chem. 17 (1988) 167-192. https://doi.org/10.1146/annurev.bb.17.060188.001123.

[30] B. Lee, F.M. Richards, The interpretation of protein structures: estimation of static accessibility, J. Mol. Biol. 55(3) (1971) 379-400.

[31] N. Desdouits, M. Nilges, A. Blondel, Principal Component Analysis reveals correlation of cavities evolution and functional motions in proteins, J. Mol. Graph. Model. 55 (2015) 13-24. https://doi.org/10.1016/j.jmgm.2014.10.011.

[32] G.M. Morris, R. Huey, W. Lindstrom, M.F. Sanner, R.K. Belew, D.S. Goodsell, A.J. Olson, AutoDock4 and AutoDockTools4: Automated docking with selective receptor flexibility, J. Comput. Chem. 30(16) (2009) 2785-2791. https://doi.org/10.1002/jcc.21256.

[33] S. Shityakov, C. Forster, *In silico* predictive model to determine vector-mediated transport properties for the blood-brain barrier choline transporter, Adv. Appl. Bioinform. Chem. 7 (2014) 23-36. https://doi.org/10.2147/aabc.s63749.

[34] R.A. Laskowski, M.B. Swindells, LigPlot+: multiple ligand-protein interaction diagrams for drug discovery, J. Chem. Inf. Model. 51(10) (2011) 2778-2786. https://doi.org/10.1021/ci200227u.

[35] N. Guex, M.C. Peitsch, SWISS-MODEL and the Swiss-PdbViewer: an environment for comparative protein modeling, Electrophoresis 18(15) (1997) 2714-2723. https://doi.org/10.1002/elps.1150181505.

[36] M. Dixon, The determination of enzyme inhibitor constants, Biochem. J. 55(1) (1953) 170-171.

[37] J.R. Lorsch, D. Herschlag, The DEAD box protein eIF4A. 1. A minimal kinetic and thermodynamic framework reveals coupled binding of RNA and nucleotide, Biochemistry 37(8) (1998) 2180-2193. https://doi.org/10.1021/bi972430g.

[38] S.P. Ryder, M.I. Recht, J.R. Williamson, Quantitative analysis of protein-RNA interactions by gel mobility shift, Methods Mol. Biol. 488 (2008) 99-115. https://doi.org/10.1007/978-1-60327-475-3_7.

[39] G. Lemaire, L. Gold, M. Yarus, Autogenous translational repression of bacteriophage T4 gene 32 expression *in vitro*, J. Mol. Biol. 126(1) (1978) 73-90.

[40] C.F. Brayton, Dimethyl sulfoxide (DMSO): a review, Cornell Vet. 76(1) (1986) 61-90.

[41] C. Monder, Discussion: effect of DMSO on enzyme activity, Ann. N. Y. Acad. Sci. 141(1) (1967) 300-301.

[42] D.H. Rammler, The effect of DMSO on several enzyme systems, Ann. N. Y. Acad. Sci. 141(1) (1967) 291-299.

[43] D.H. Rammler, A. Zaffaroni, Biological implications of DMSO based on a review of its chemical properties, Ann. N. Y. Acad. Sci. 141(1) (1967) 13-23.

[44] A. Pabbathi, S. Patra, A. Samanta, Structural transformation of bovine serum albumin induced by dimethyl sulfoxide and probed by fluorescence correlation spectroscopy and additional methods, Chemphyschem 14(11) (2013) 2441-2449. https://doi.org/10.1002/cphc.201300313.

[45] S. Dupont, G. Lemetais, T. Ferreira, P. Cayot, P. Gervais, L. Beney, Ergosterol biosynthesis: a fungal pathway for life on land?, Evolution 66(9) (2012) 2961-2968. https://doi.org/10.1111/j.1558-5646.2012.01667.x.

[46] H. Dixon, C.D. Ginger, J. Williamson, Trypanosome sterols and their metabolic origins, Comp. Biochem. Physiol. B 41(1) (1972) 1-18.

[47] S.T. de Macedo-Silva, W. de Souza, J.C. Rodrigues, Sterol Biosynthesis Pathway as an Alternative for the Anti-Protozoan Parasite Chemotherapy, Curr. Med. Chem. 22(18) (2015) 2186-2198.

[48] D.G. Sant, S.G. Tupe, C.V. Ramana, M.V. Deshpande, Fungal cell membrane-promising drug target for antifungal therapy, J. Appl. Microbiol. 121(6) (2016) 1498-1510. https://doi.org/10.1111/jam.13301.

[49] S. Fouace, L. El kihel, M. Dherbomez, Y. Letourneux, Stereoselective synthesis of 7 alpha- and 7 beta-aminocholestanol as potent fungicidal drugs, Bioorg. Med. Chem. Lett. 11(23) (2001) 3011-3014.

[50] N.K. Tanner, O. Cordin, J. Banroques, M. Doere, P. Linder, The Q motif: a newly identified motif in DEAD box helicases may regulate ATP binding and hydrolysis, Mol. Cell 11(1) (2003) 127-138.